A novel gold nanoparticles decorated nanocrystalline zeolite based electrochemical sensor for the nanomolar simultaneous detection of cysteine and glutathione

Balwinder Kaur, Rajendra Srivastava*, and Biswarup Satpati

Supporting Information

Chronoamperometry study

Chronoamperometry was used to calculate the diffusion coefficient (D) and rate constant (k) for the electrocatalytic reaction (Fig. S8-S9). Chronoamperograms were obtained at different concentrations of analytes at a desired potential step (350 and 580 mV for CySH and GSH, respectively) (Fig. S8-S9). The plots of I verses $t^{-1/2}$ exhibited straight lines for different concentrations of analytes (Fig. S8-S9, inset a). Cottrell equation (Eq. 1) was used to calculate the diffusion coefficient for various analytes investigated in this study.[1]

$$I_p = n\,F\,A\,D^{1/2}\,c/\pi^{1/2}\,t^{1/2} \qquad (1)$$

Where I_p is the catalytic current of AuNPs(0.5%)-Nano-ZSM-5/GCE in the presence of analyte, F is the Faraday constant (96485 C/mole), A is the geometric surface area of the electrode (0.07 cm^2), D is the diffusion coefficient (cm^2/s), c is the analyte concentration (mol/cm^3), and t is the time elapsed (s). The diffusion coefficients were found to be 3.1×10^{-5} and 1.4×10^{-5} cm^2/s for CySH and GSH, respectively.

Chronoamperometry was also employed to calculate the rate constant (k) for electro-catalytic reaction through Eq. 2. [2]

$$I_C/I_L = \gamma^{1/2}\,[\pi^{1/2}\,\mathrm{erf}\,(\gamma^{1/2}) + \exp\,(-\gamma)/\gamma^{1/2}] \qquad (2)$$

Where I_C is the catalytic current of AuNPs(0.5%)-Nano-ZSM-5/GCE in the presence of analyte, I_L is the limiting current in the absence of analyte and $\gamma = kC_0t$ (C_0 is the bulk concentration of analyte) is the argument of the error function. In cases, where γ exceed 2, the error function is almost equal to 1 and the above equation can be reduced to:

$$I_C/I_L = \pi^{1/2}\,\gamma^{1/2} = \pi^{1/2}\,(kct)^{1/2} \qquad (3)$$

Where k, c and t are the catalytic rate constant (1/M s), analyte concentration (M), and time elapsed (s), respectively. Eq. 3 can be used to calculate the rate constant of the catalytic process. Based on the slope of I_C/I_L vs. $t^{1/2}$ plot; k can be obtained for a given analyte concentration (Fig. S8-S9, inset b). From the values of the slopes, an average value for k was obtained for the

oxidation of analyte. The rate constant values for electro-catalytic oxidation of CySH and GSH were found as 17.0×10^3 and 3.2×10^3 1/s M, respectively.

FT-IR investigation of synthesized materials

Fig. S1 shows the FT-IR spectra of Nano-ZSM-5 and Nano-ZSM-5-Pr-NH_2 samples. Nano-ZSM-5 exhibited several common IR peaks at 800 cm^{-1}, 970 cm^{-1}, 1100 cm^{-1}, and 1230 cm^{-1} (Fig. S1).[3] The absorption peak at 800 cm^{-1} is due to Si−O−Si symmetric stretching.[4] The absorption peaks at 1100 cm^{-1} and 1230 cm^{-1} are assigned to asymmetric stretching of Si−O−Si whereas peak at 970 cm^{-1} is due to the incorporation of Al in the MFI framework and assigned to an asymmetric stretching mode of a [SiO_4] unit bonded to a M^{4+} ion (O_3Si–O–M). Nano-ZSM-5-Pr-NH_2 exhibited IR peaks at 2930 and 2842 cm^{-1}, which are characteristics of asymmetric and symmetric –CH_2 stretching vibrations in the propyl chain, respectively.[4] The absorption bands at 1596 and 1410 cm^{-1} are assigned to the bending mode of the -NH_2 group and to the scissor vibration of -NH, respectively. The absorption band at 1470 cm^{-1} is due to –CH_2 bending (scissoring) vibration. The C-N stretching frequency for the aminopropyl moiety is observed at 1189 cm^{-1}. These observations confirmed the incorporation of propylamine moiety on the surface of Nano-ZSM-5.

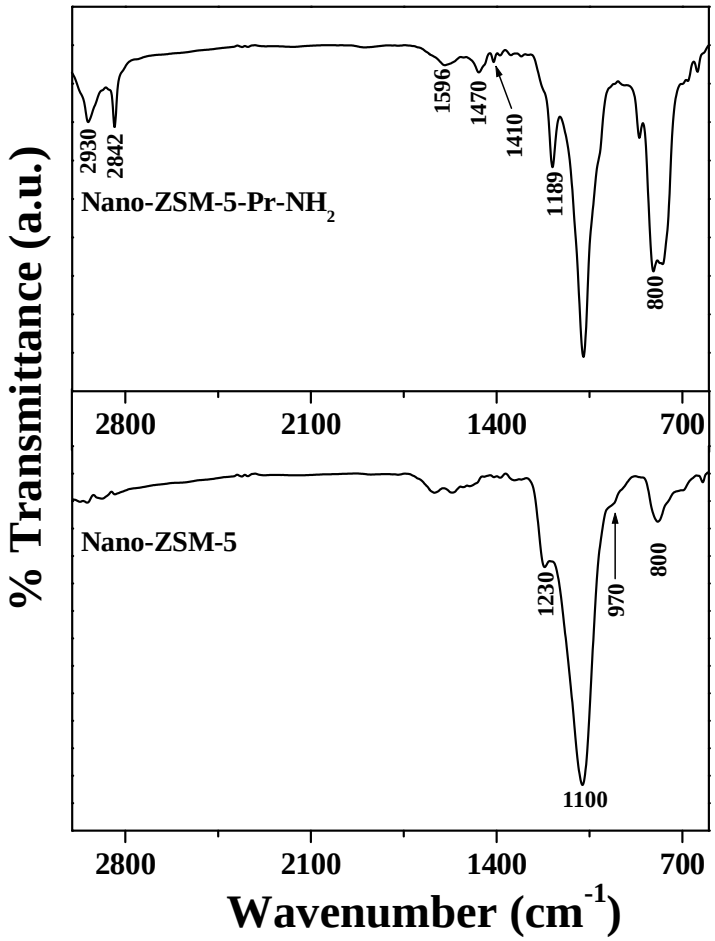

Figure S1. FT-IR spectra of Nano-ZSM-5 and Nano-ZSM-5-Pr-NH_2 materials investigated in the study.

TGA investigation of synthesized materials

Fig. S2 shows the TGA curves for Nano-ZSM-5 and Nano-ZSM-5-Pr-NH_2. The first weight loss below 473 K in the TGA curves for both the samples indicates the loss of physically adsorbed water molecules. The TGA curve for Nano-ZSM-5 showed no appreciable weight loss after 473 K, confirming that chemical composition did not change in this temperature range. In the TGA curve for Nano-ZSM-5-Pr-NH_2, the second weight loss between 525 K-875 K can be attributed to the decomposition of organic propylamine moiety anchored on the surface of Nano-ZSM-5 and the residual weight refers to the content of Nano-ZSM-5 in Nano-ZSM-5-Pr-NH_2. TGA analysis confirmed that Nano-ZSM-5-Pr-NH_2 contains 11 wt % functionalized organic group (-Pr-NH_2).

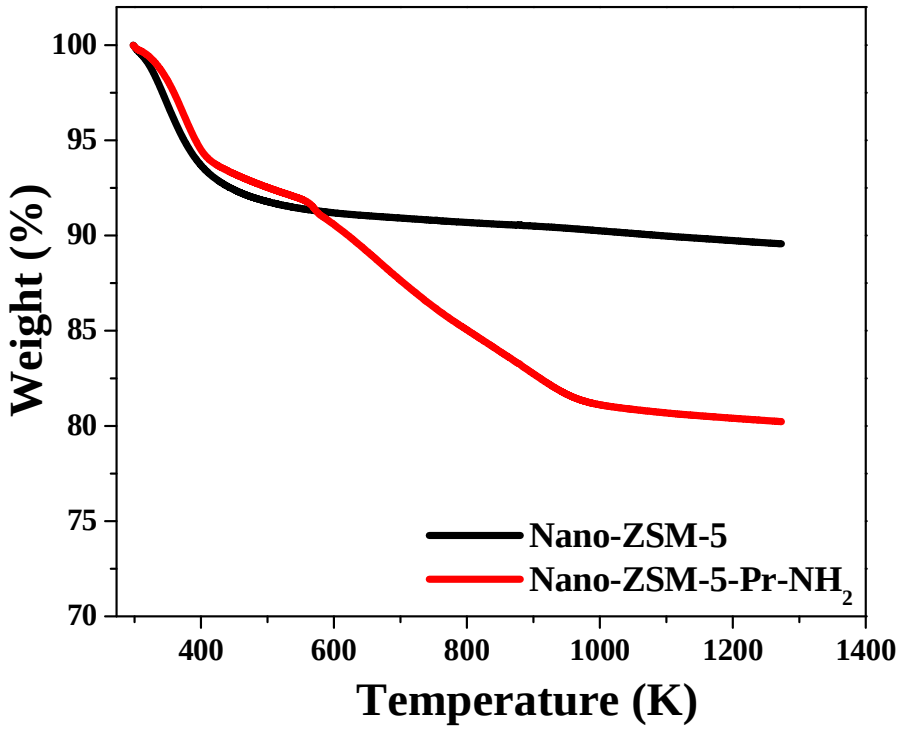

Figure S2. TGA thermograms of Nano-ZSM-5 and Nano-ZSM-5-Pr-NH_2 at a heating rate of 10 K/min recorded in air stream.

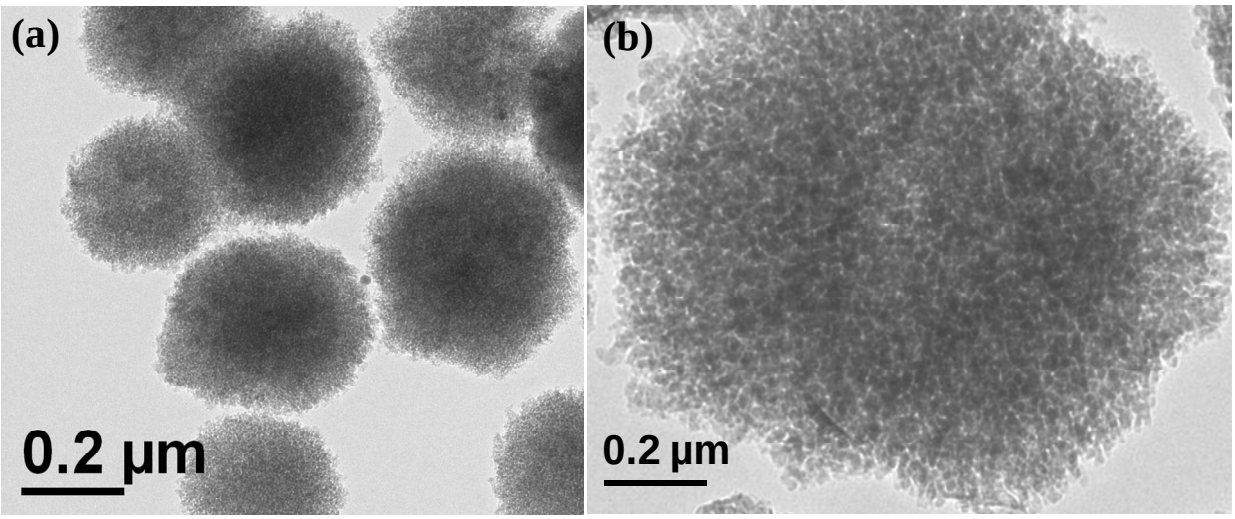

Figure S3. (a) TEM image and (b) high resolution TEM image of Nano-ZSM-5.

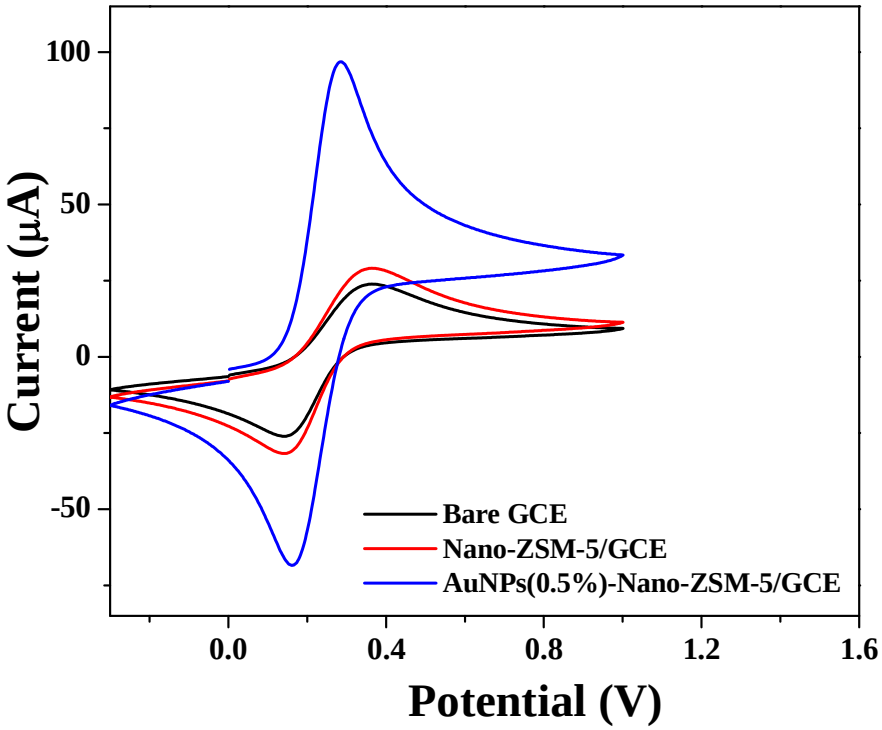

Figure S4. CV responses at AuNPs(0.5%)-Nano-ZSM-5/GCE, Nano-ZSM-5/GCE and bare GCE in 0.1 M KCl solution containing 10 mM of $[Fe(CN)_6]^{3-/4-}$ at a scan rate of 10 mV/s.

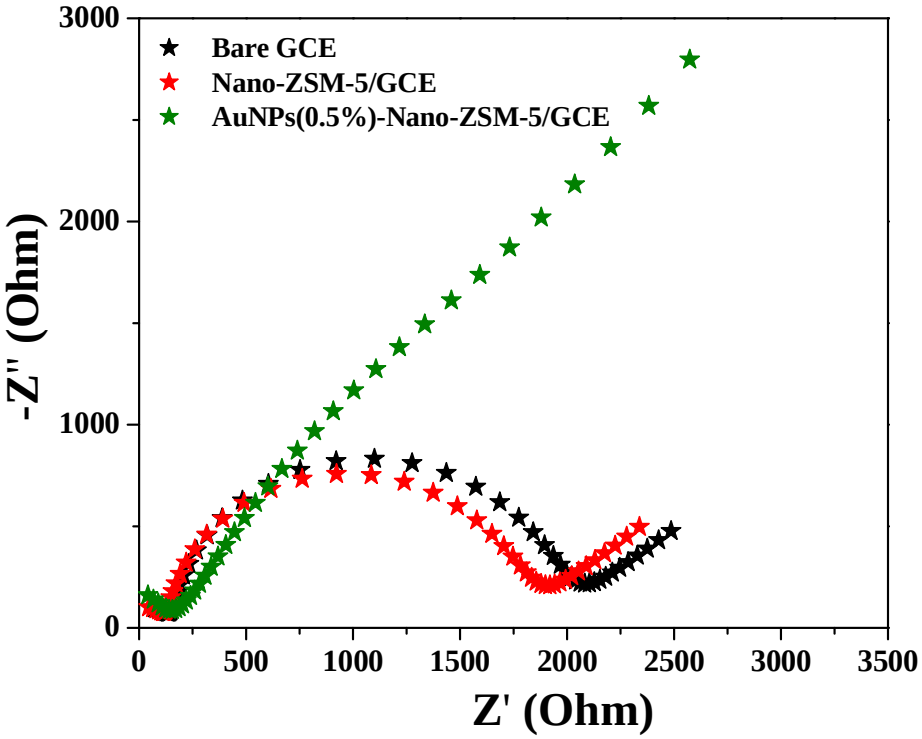

Figure S5. Nyquist plots of impedance profiles at AuNPs(0.5%)-Nano-ZSM-5/GCE, Nano-ZSM-5/GCE, and bare GCE in 0.1 M KCl solution containing 10 mM $[Fe(CN)_6]^{3-/4-}$ over the frequency range from 0.1 Hz to 10^5 Hz at an applied potential of 0.3 V.

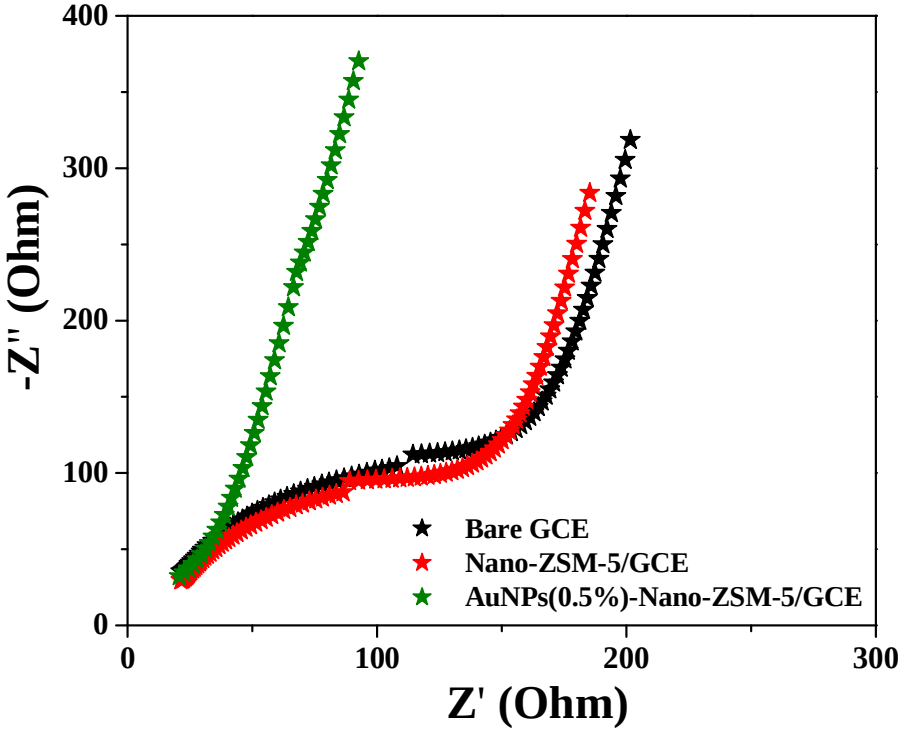

Figure S6. Nyquist plots of impedance profiles at AuNPs(0.5%)-Nano-ZSM-5/GCE, Nano-ZSM-5/GCE, and bare GCE in 0.1 M KCl solution containing 10 mM $[Fe(CN)_6]^{3-/4-}$ over the frequency range from 0.1 Hz to 10^6 Hz at an applied potential of 0.3 V.

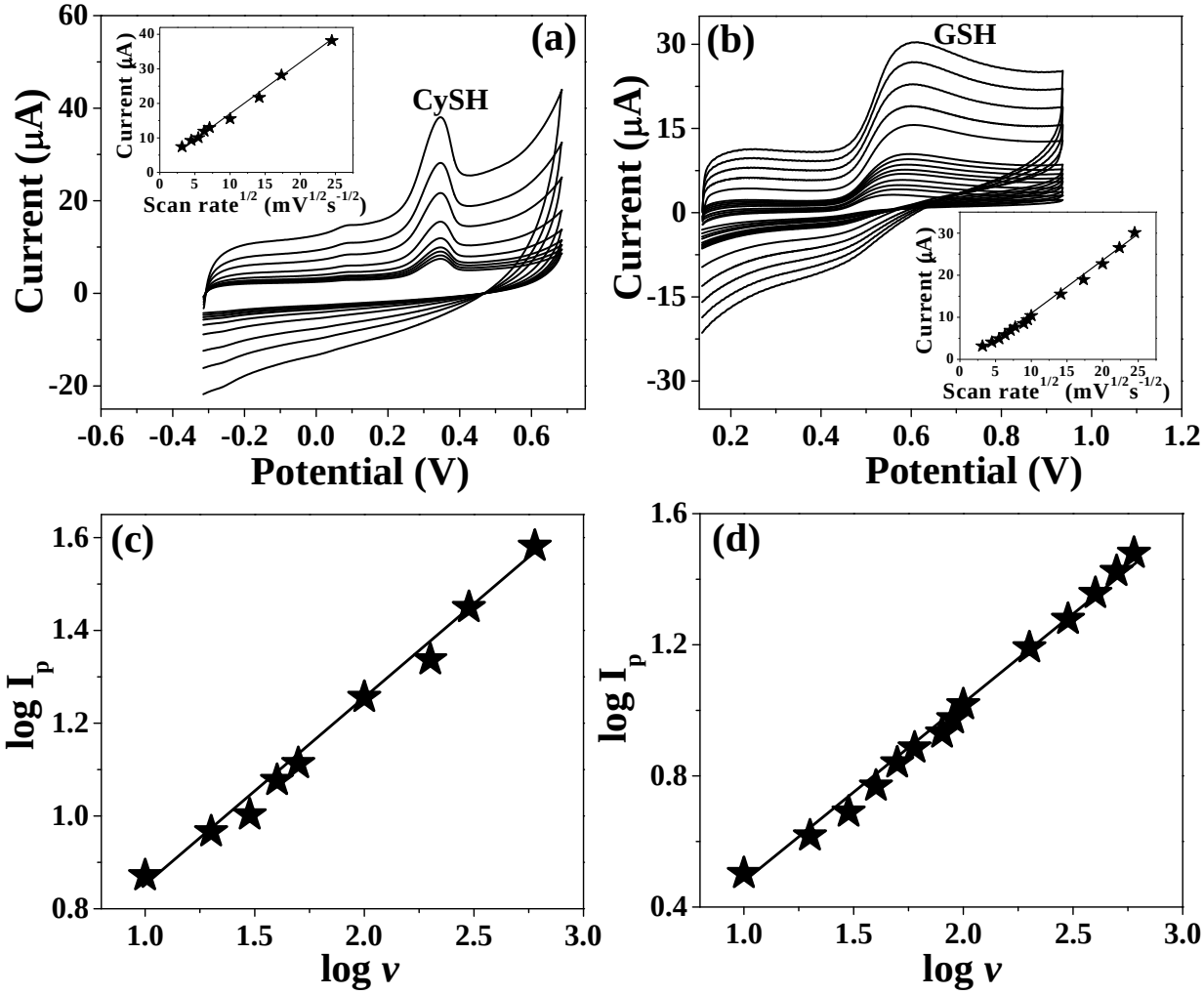

Figure S7. CVs at AuNPs(0.5%)-Nano-ZSM-5/GCE containing (a) CySH (10 μM), (b) GSH (10 μM) in 0.1 M PBS (pH 7.4) at various scan rates (10-600 mV/s). Inset shows the plot of oxidation peak currents vs. square root of scan rates. (c)-(d) Plot of log I_p and log scan rate (ν) for the electrochemical oxidation of (c) CySH, and (d) GSH at AuNPs(0.5%)-Nano-ZSM-5/GCE.

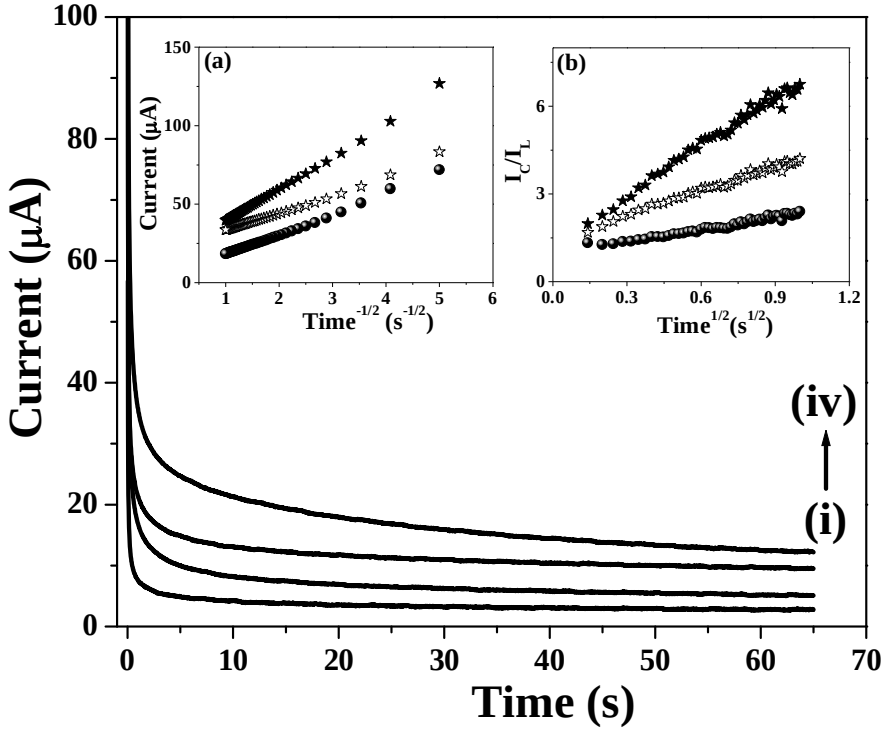

Figure S8. Chronoamperograms obtained at AuNPs(0.5%)-Nano-ZSM-5/GCE (i) in the absence and in the presence of (ii) 100 μM, (iii) 200 μM, and (iv) 300 μM of CySH in 10 mL 0.1 M PBS (pH 7.4). Inset: (a) Dependence of current on the time$^{-1/2}$ derived from the chronoamperogram data. (b) Dependence of I_C/I_L on time$^{1/2}$ derived from the data of chronoamperograms.

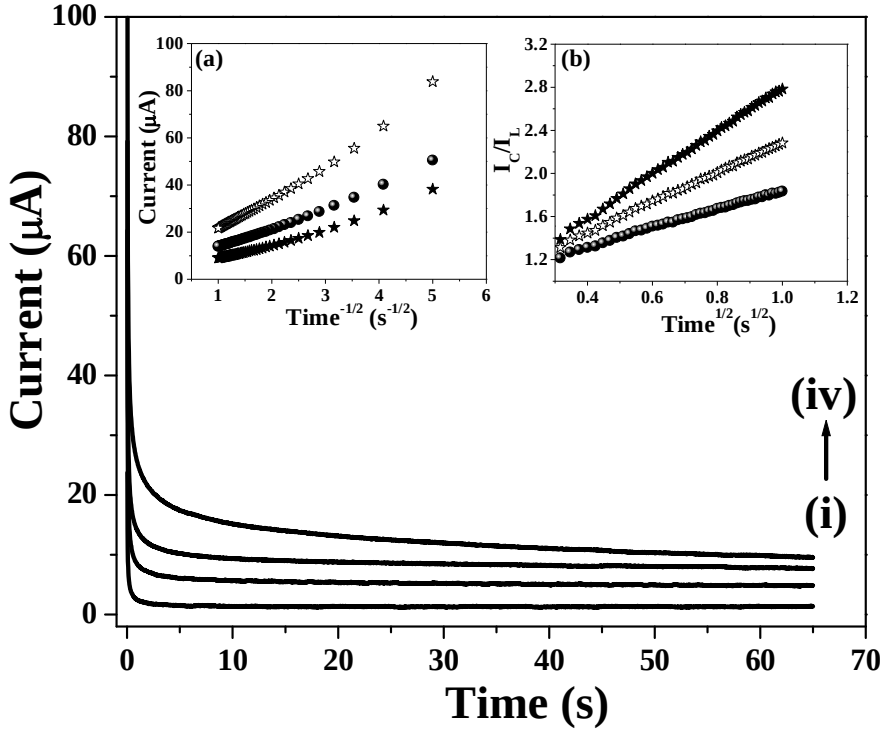

Figure S9. Chronoamperograms obtained at AuNPs(0.5%)-Nano-ZSM-5/GCE (i) in the absence and in the presence of (ii) 100 μM, (iii) 200 μM, and (iv) 300 μM of GSH in 10 mL 0.1 M PBS (pH 7.4). Inset: (a) Dependence of current on the time$^{-1/2}$ derived from the chronoamperogram data. (b) Dependence of I_C/I_L on time$^{1/2}$ derived from the data of chronoamperograms.

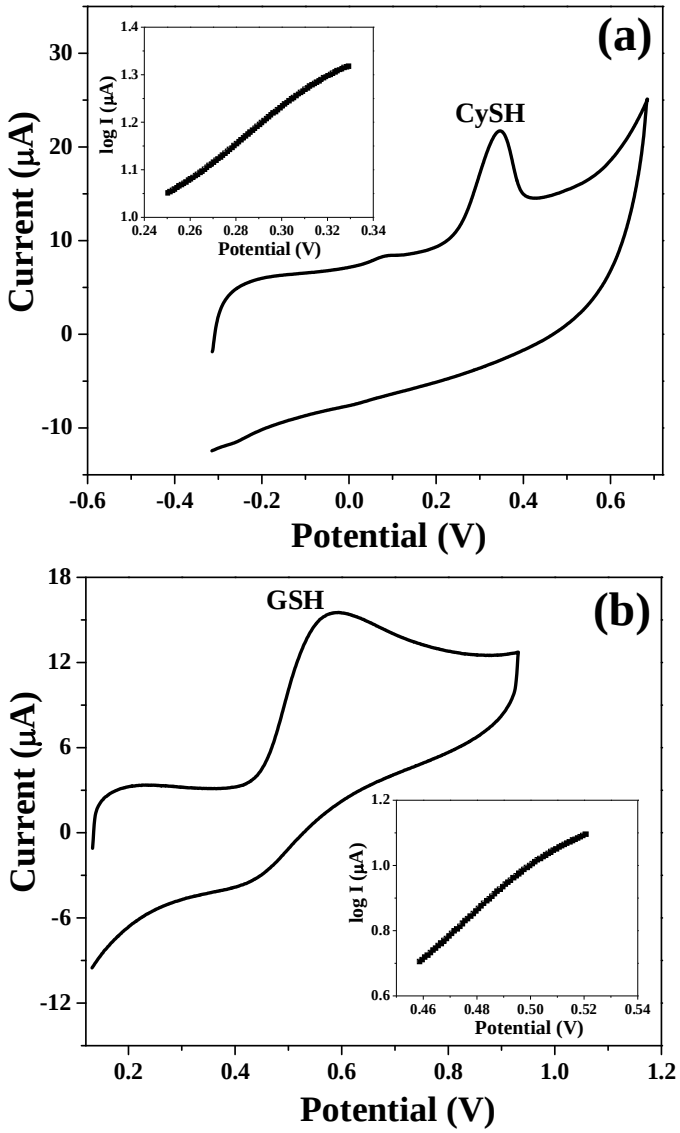

Figure S10. CVs of AuNPs(0.5%)-Nano-ZSM-5/GCE in the presence of (a) CySH (10 μM) and (b) GSH (10 μM) in 0.1 M PBS (pH 7.4) at a scan rate of 50 mV/s. Inset shows the tafel plot of CV for (a) CySH and (b) GSH at AuNPs(0.5%)-Nano-ZSM-5/GCE.

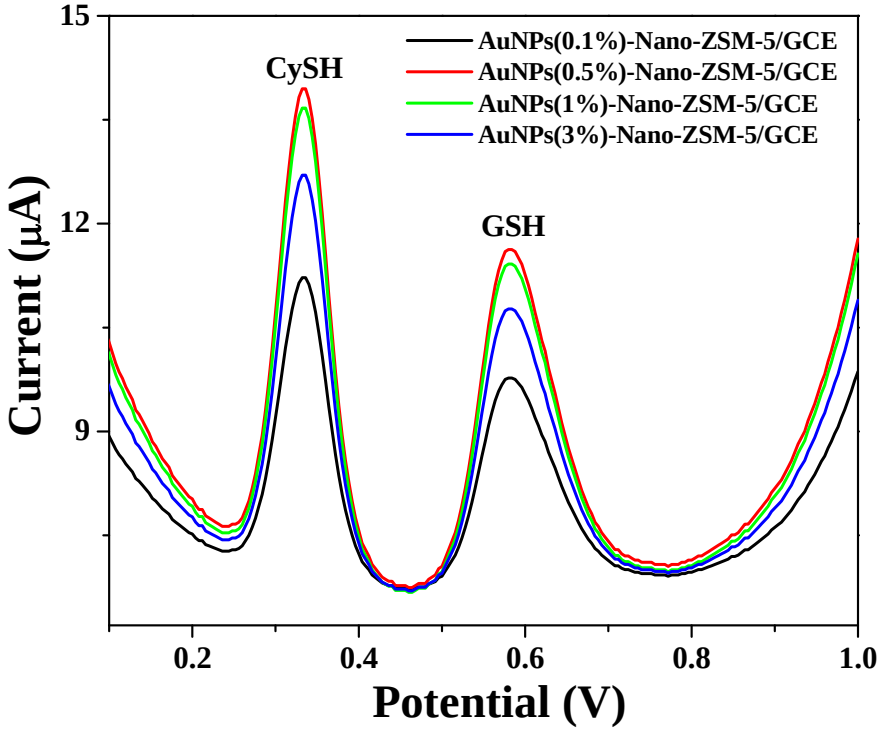

Figure S11. DPVs in the presence of 1 μM each of CySH and GSH in 10 mL of 0.1 M PBS (pH 7.4) at AuNPs(0.1%)-Nano-ZSM-5/GCE, AuNPs(0.5%)-Nano-ZSM-5/GCE, AuNPs(1%)-Nano-ZSM-5/GCE, and AuNPs(3%)-Nano-ZSM-5/GCE. DPV parameters were selected as: pulse amplitude: 50 mV, pulse width: 50 ms, scan rate: 20 mV/s.

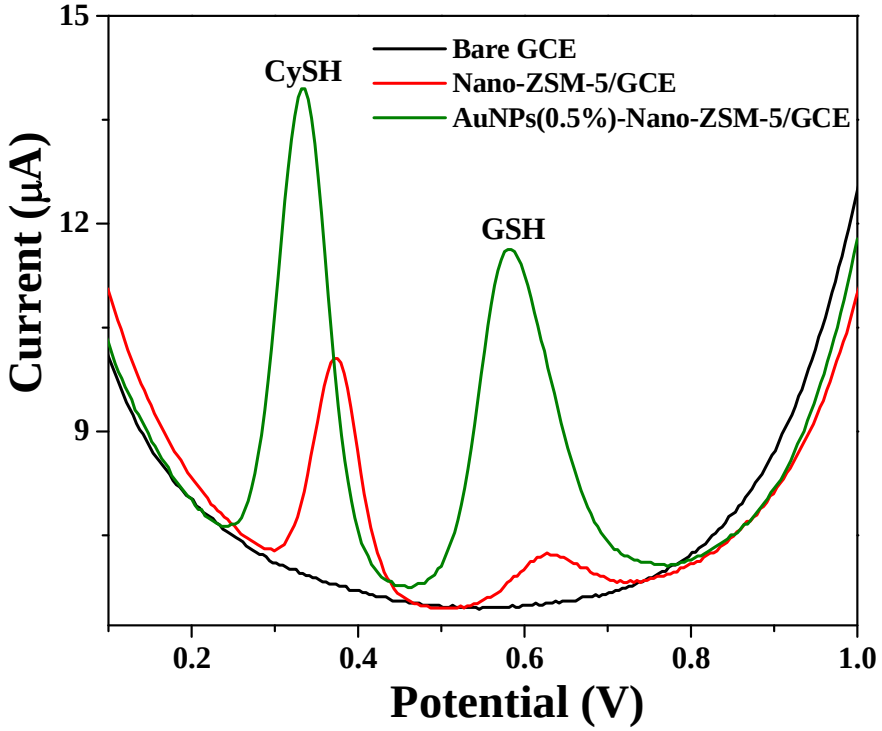

Figure S12. Comparison of DPV of binary mixture containing 1 μM each of CySH and GSH at AuNPs(0.5%)-Nano-ZSM-5/GCE, Nano-ZSM-5/GCE, and bare GCE in 0.1 M PBS (pH 7.4). DPV parameters were selected as: pulse amplitude: 50 mV, pulse width: 50 ms, scan rate: 20 mV/s.

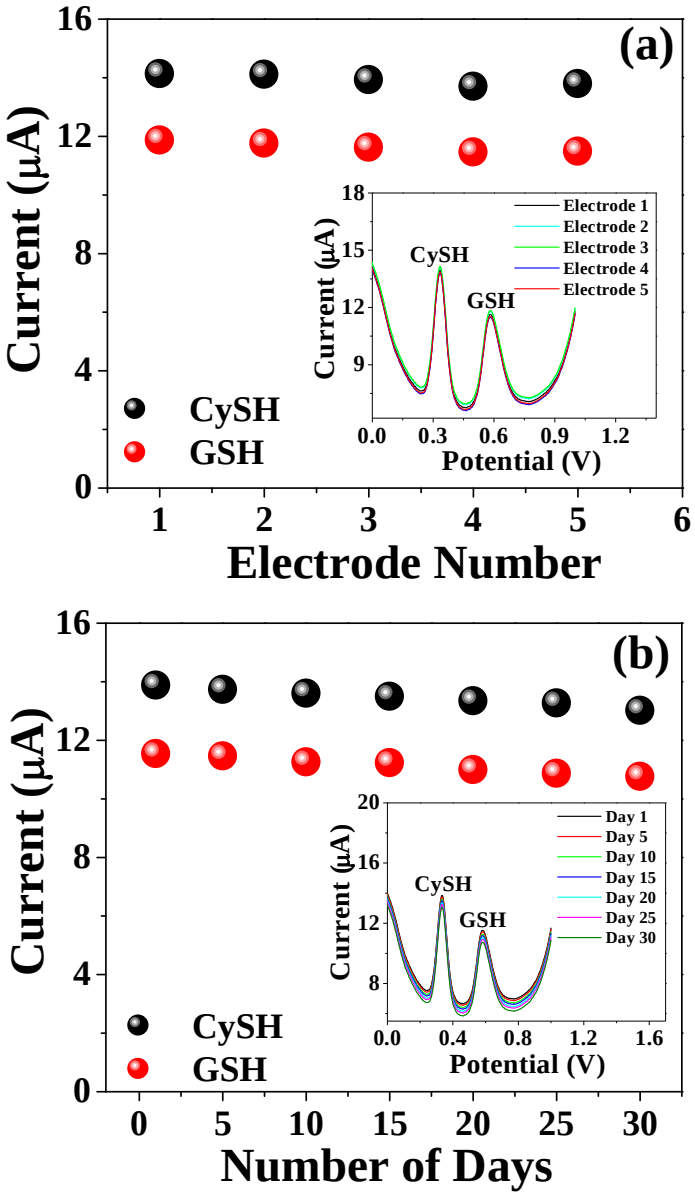

Figure S13. The current response in the presence of 1 μM each of CySH and GSH (a) at different freshly prepared Au(0.5%)-Nano-ZSM-5/GCEs (n=5). Inset shows corresponding DPV curves at 5 different Au(0.5%)-Nano-ZSM-5/GCEs in the presence of 1 μM each of CySH and GSH and (b) at seven different measurements (30 days time period at the interval of every 5 days) using same Au(0.5%)-Nano-ZSM-5/GCE. Inset shows corresponding DPV curves at 7 different measurements using same Au(0.5%)-Nano-ZSM-5/GCE in the presence of in the presence of 1 μM each of CySH and GSH for 30 days time period at the interval of every 5 days.

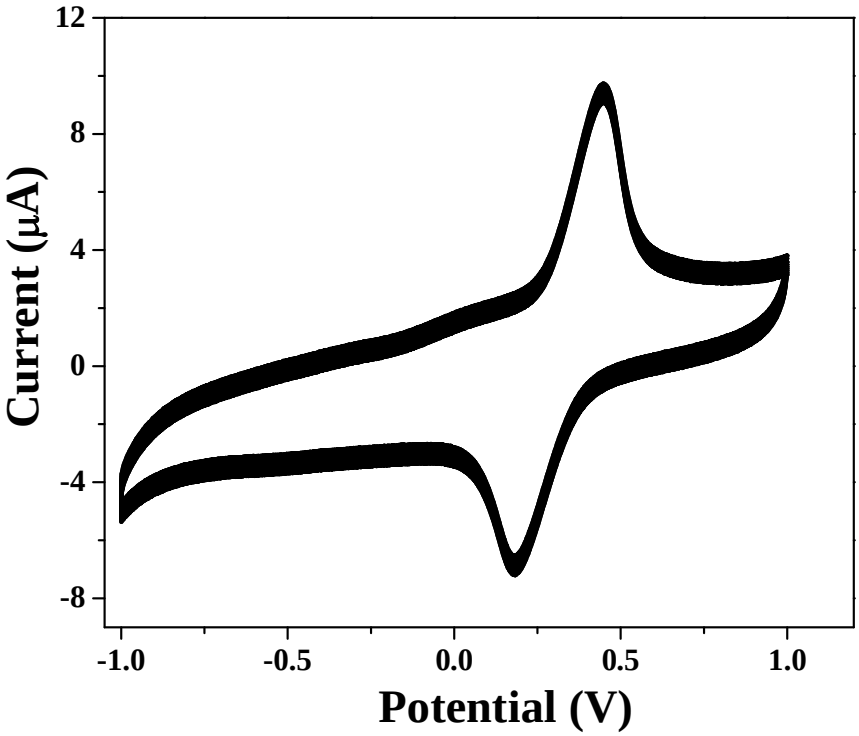

Figure S14. CVs for 50 cycles at AuNPs(0.5%)-Nano-ZSM-5/GCE at in 0.1 M PBS (pH 7.4) at a scan rate of 50 mV/s.

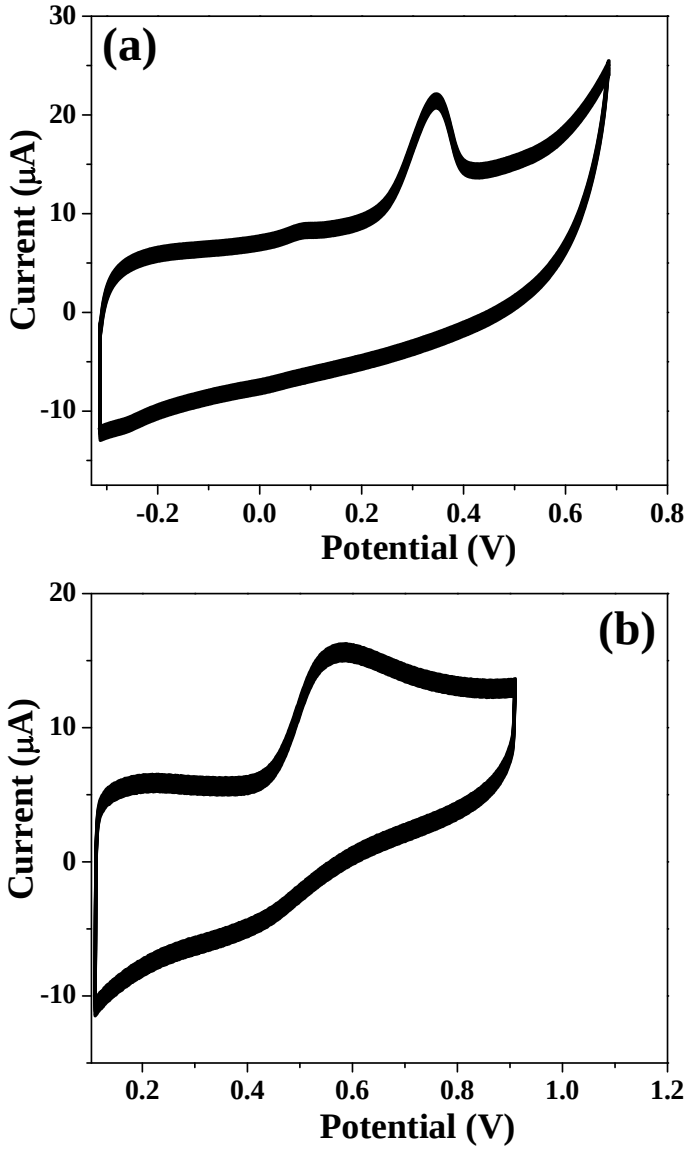

Figure S15. CVs for 50 cycles at AuNPs(0.5%)-Nano-ZSM-5/GCE at a scan rate 50 mV/s in 0.1 M PBS (pH 7.4) in the presence of (a) CySH (10 μM) and (b) GSH (10 μM).

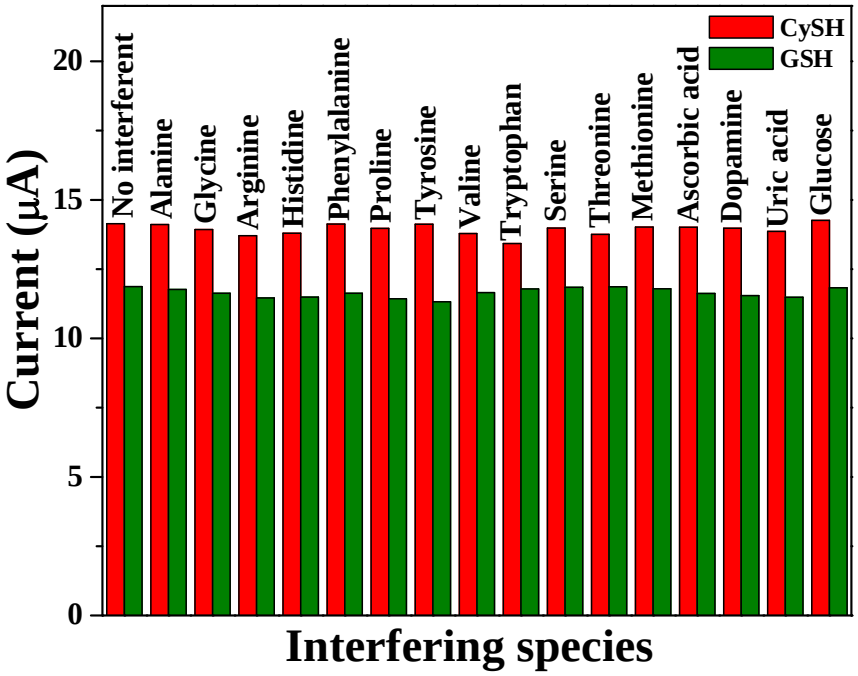

Figure S16. DPV responses of AuNPs(0.5%)-Nano-ZSM-5/GCE in 0.1 M PBS (pH 7.4) containing 1 μM each of CySH and GSH in the absence and in the presence of 500 μM each of different interfering species. DPV parameters were selected as: pulse amplitude: 50 mV, pulse width: 50 ms, scan rate: 20 mV/s.

Table S1. Comparison of Au(0.5%)-Nano-ZSM-5/GCE with other electrodes reported in the literature for CySH and GSH detection.

S.No.	Electrode material	Analyte	Linear range (M)	Detection limit (M)	Reference
1.	Cyclotricatechylene	CySH	0 μM – 40 μM	0.6 μM	[5]
2.	Sb-doped ZnO nanowires	CySH	75 nM – 100 μM	25 nM	[6]
3.	Manganese dioxide-carbon nanocomposite	CySH	0.5 μM – 680 μM	22 nM	[7]
4.	MWCNTs/gold nanorods	CySH	5 μM – 200 μM	8.25 nM	[8]
5.	Graphene oxide/Au nanocluster	CySH	50 nM – 20 μM	20 nM	[9]
6.	Ce-doped Mg–Al layered double hydroxide	CySH	10 μM – 5400 μM	4.2 μM	[10]
7.	Manganese vanadate nanorods	CySH	50 nM – 2 mM	26 nM	[11]
8.	FePt/CNTs nanocomposite	GSH	80 nM – 220 μM	50 nM	[12]
9.	Cu_2O/NiO_x/graphene oxide	GSH	2 μM – 1.3 mM	300 nM	[13]
10.	Co-based metal-organic polymer	GSH	2.5 μM – 950 μM	2.5 μM	[14]
11.	Cobalt phthalocyanine –nitrogen doped graphene	CySH GSH	1 μM – 16 mM 1 μM – 16 mM	1 μM 1 μM	[15]
12.	Au(5%)-Nano-ZSM-5	CySH GSH	2 nM – 800 μM 3 nM – 800 μM	0.3 nM 0.6 nM	This work

References

1. M. Sharp, M. Petersson and K. Edström, *J. Electroanal. Chem.*, 1979, **95**, 123-130.
2. Z. Galus, G. Reynolds and S. Marcinkiewicz, *Fundamentals of electrochemical analysis, Ellis Horwood Chichester*, 1976, **328**.
3. P. Ratnasamy, D. Srinivas and H. Knözinger, *Adv. Catal.*, 2004, **48**, 1-169.
4. D. Jung, C. Streb and M. Hartmann, *Int. J. Mol. Sci.*, 2010, **11**, 762-778.
5. P. T. Lee, J. E. Thomson, A. Karina, C. Salter, C. Johnston, S. G. Davies and R. G. Compton, *Analyst*, 2015, **140**, 236-242.
6. M. Ahmad, C. Pan and J. Zhu, *J. Mater. Chem.*, 2010, **20**, 7169-7174.
7. C. Xiao, J. Chen, B. Liu, X. Chu, L. Wu and S. Yao, *PCCP*, 2011, **13**, 1568-1574.
8. F. d. A. dos Santos Silva, M. G. A. da Silva, P. R. Lima, M. R. Meneghetti, L. T. Kubota and M. O. F. Goulart, *Biosens. Bioelectron.*, 2013, **50**, 202-209.
9. S. Ge, M. Yan, J. Lu, M. Zhang, F. Yu, J. Yu, X. Song and S. Yu, *Biosens. Bioelectron.*, 2012, **31**, 49-54.
10. Y. Wang, W. Peng, L. Liu, F. Gao and M. Li, *Electrochim. Acta*, 2012, **70**, 193-198.
11. L. Pei, Y. Pei, Y. Xie, C. Fan and H. Yu, *CrystEngComm*, 2013, **15**, 1729-1738.
12. R. Moradi, S. Sebt, H. Karimi-Maleh, R. Sadeghi, F. Karimi, A. Bahari and H. Arabi, *PCCP*, 2013, **15**, 5888-5897.
13. B. Yuan, C. Xu, L. Liu, Q. Zhang, S. Ji, L. Pi, D. Zhang and Q. Huo, *Electrochim. Acta*, 2013, **104**, 78-83.
14. B. Yuan, R. Zhang, X. Jiao, J. Li, H. Shi and D. Zhang, *Electrochem. Commun.*, 2014, **40**, 92-95.
15. H. Xu, J. Xiao, B. Liu, S. Griveau and F. Bedioui, *Biosens. Bioelectron.*, 2015, **66**, 438-444.